# Supporting Information for "The 2020 $M_w$ 6.5 Monte Cristro Range (Nevada) earthquake: anatomy of a large rupture through a region of highly-distributed faulting"

I. Sethanant[1], E. Nissen[1], L. Pousse-Beltran[1,2], E. Bergman[3], I. Pierce[4]

[1]School of Earth and Ocean Sciences, University of Victoria, British Columbia, Canada

[2]Institut des Sciences de la Terre, Université Grenoble Alpes, Université Savoie Mont Blanc, CNRS, IRD, 38000 Grenoble, France

[3]Global Seismological Services, Golden, Colorado, USA

[4]Department of Earth Sciences, University of Oxford, United Kingdom

**Contents of this file**

1. Figure A1: Observed versus modeled surface displacements

2. Figure A2: Comparison of the centroid and focal depths

3. Figure A3: Relative and absolute location results from *mloc*

4. Figure A4: Theoretical and observed arrival time data

5. Figure A5: Arrival times from various scales of epicentral distances

6. Table B1: Velocity model used in the *mloc* relocation

**Additional Supporting Information (Files uploaded separately)**

––––––––

Corresponding author: I. Sethanant, School of Earth and Ocean Sciences, University of Victoria, British Columbia, Canada. (isethanant@uvic.ca)

July 15, 2022, 11:22pm

1. Data file C1: Parameters of the distributed slip model sub-fault patches

2. Data file C2: *mloc* calibrated hypocenters

3. Data file C3: Regional moment tensor solutions

**Introduction** The Supplementary Information includes five figures (Figures A1–A5), one table (Figure B1), and three long tables (Tables C1–C3) uploaded separately. The figures show additional results from the InSAR-GNSS inversion and seismological modeling. Tables in the Supplementary Information and data files include the velocity model used in the earthquake relocation, and the full modeling results.

**References**

Blewitt, G., Hammond, W. C., & Kreemer, C. (2018). Harnessing the GPS data explosion for interdisciplinary science. *Eos*, *99*(10.1029), 485. doi: 10.1029/2018EO104623

Kennett, B. L. N., Engdahl, E. R., & Buland, R. (1995). Constraints on seismic velocities in the Earth from traveltimes. *Geophysical Journal International*, *122*(1), 108–124. doi: 10.1111/j.1365-246X.1995.tb03540.x
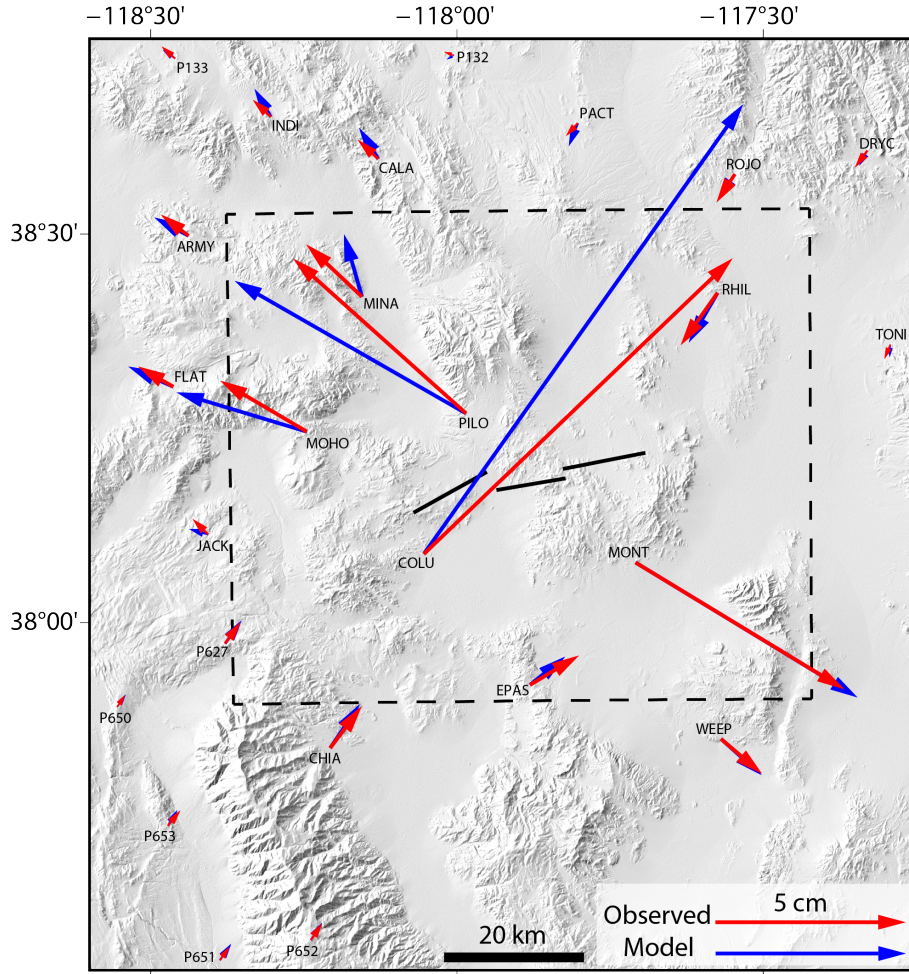
**Figure A1.**    Observed GNSS coseismic surface displacements (red vectors, labeled with station names), processed by the Nevada Geodetic Laboratory as of 19 June 2020 (Blewitt et al., 2018), and our InSAR-GNSS distributed slip model surface displacements at the same locations (blue vectors). Thick black lines show the surface projections of our preferred three model faults. The dashed box indicates the boundary of Figure 2. See Sections 3.1 and 3.2 for further details. Station locations and coseismic offsets can be found at http://geodesy.unr.edu/news_items/20200619/nn00725272_24hr_19-Jun-2020.txt.
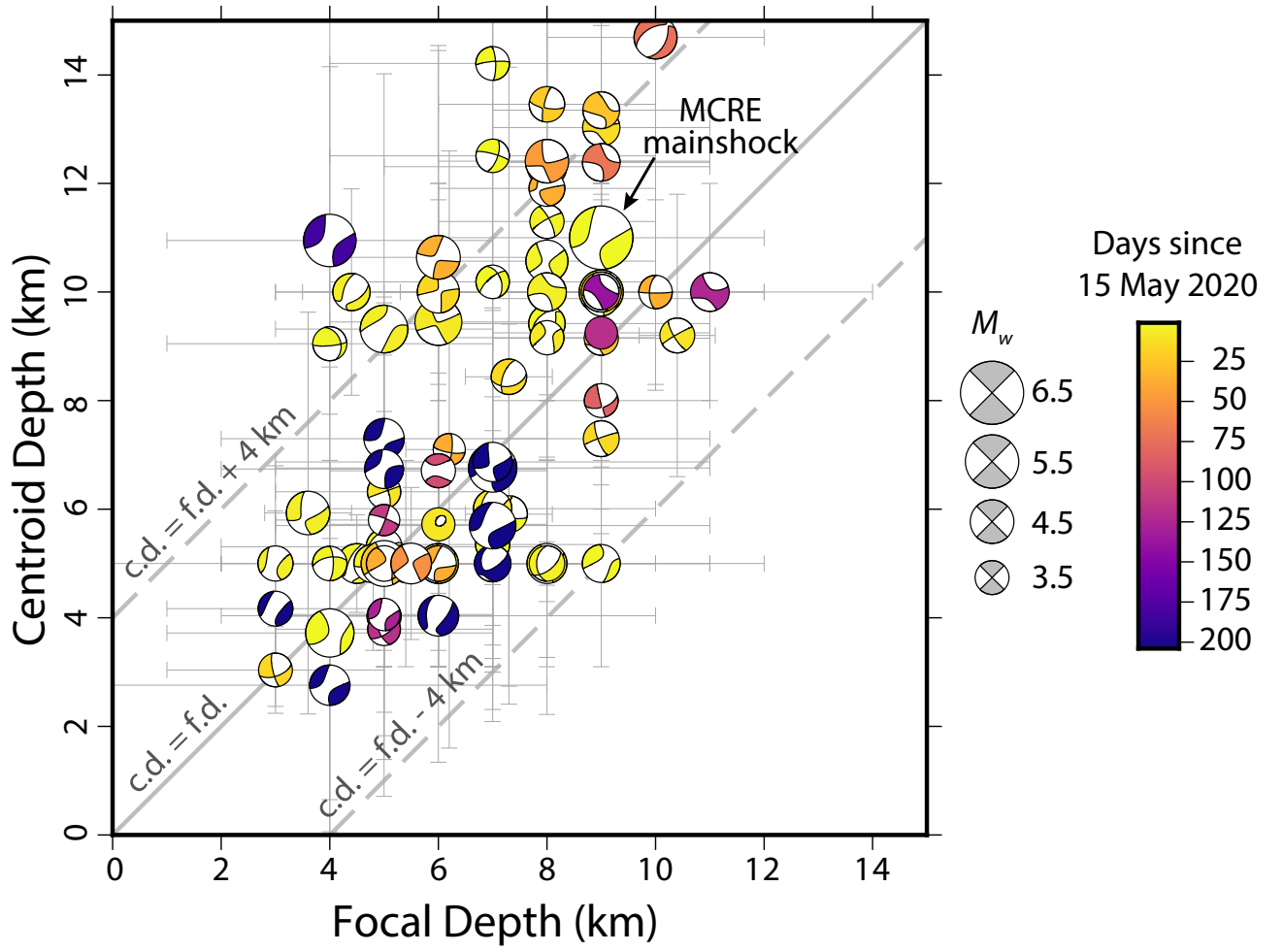
**Figure A2.** Comparison of centroid and focal depths of the 90 best-recorded events of the MCRE sequence (including the mainshock), calculated from regional waveform modeling and calibrated multi-event relocations, respectively (see Sections 3.3 and 3.4 for further details). The focal mechanisms are shaded by the number of days since 15 May 2020 (the mainshock), scaled by moment magnitude, with estimated uncertainty ranges as thin gray bars. The thicker gray line represents equality of centroid depths (c.d.) and focal depths (f.d.), and dashed gray lines denote 4 km offsets between the two.
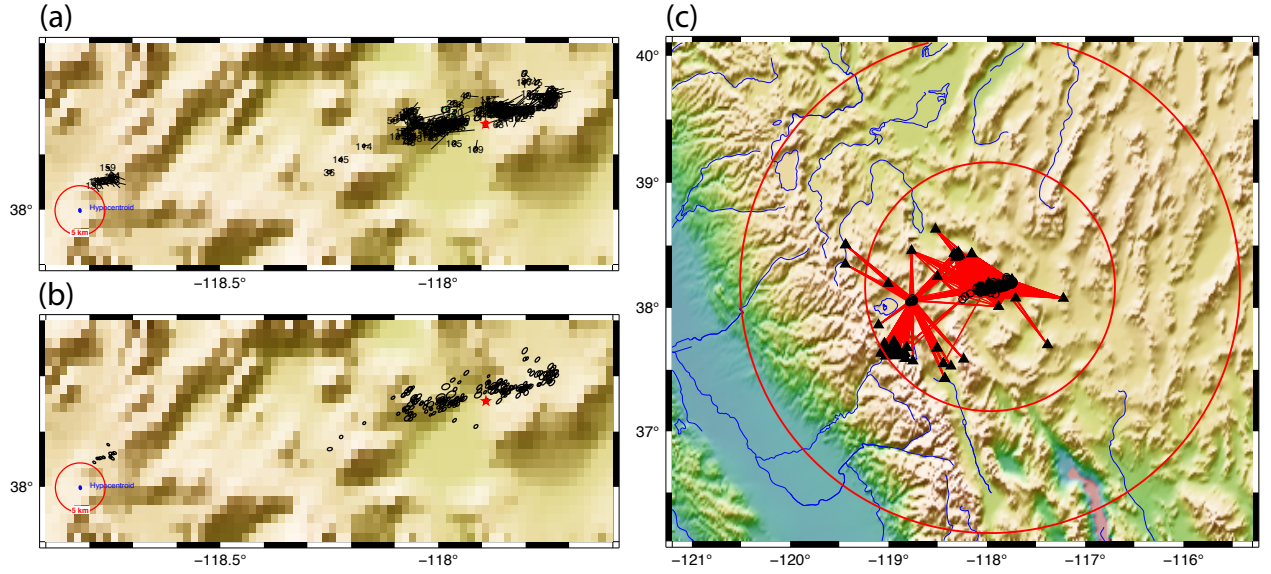
July 15, 2022, 11:22pm

**Figure A3.**   (a) Relocated epicenters (event numbers) and cluster vectors (black lines) showing the shift from starting locations to final, relative relocations. The red circle is a 5 km radius scale. (b) Similar to panel (a) but with 90% confidence ellipses. (c) Raypaths used for the direct calibration (absolute locations). Open circles are calibrated epicenters, black triangles are seismic stations, and red vectors are raypaths used for direct calibration. The two red circles show 1.0° and 2.0° radii centered upon the cluster hypocentroid. See https://seismo.com/mloc/summary-plots/ for more details.

**Table B1.**   1-D velocity model used in the *mloc* relocation, with customized phase velocities for the crust and upper mantle (<120 km) and the ak135 global model used below 120 km (Kennett et al., 1995). The Moho depth is at 30 km.

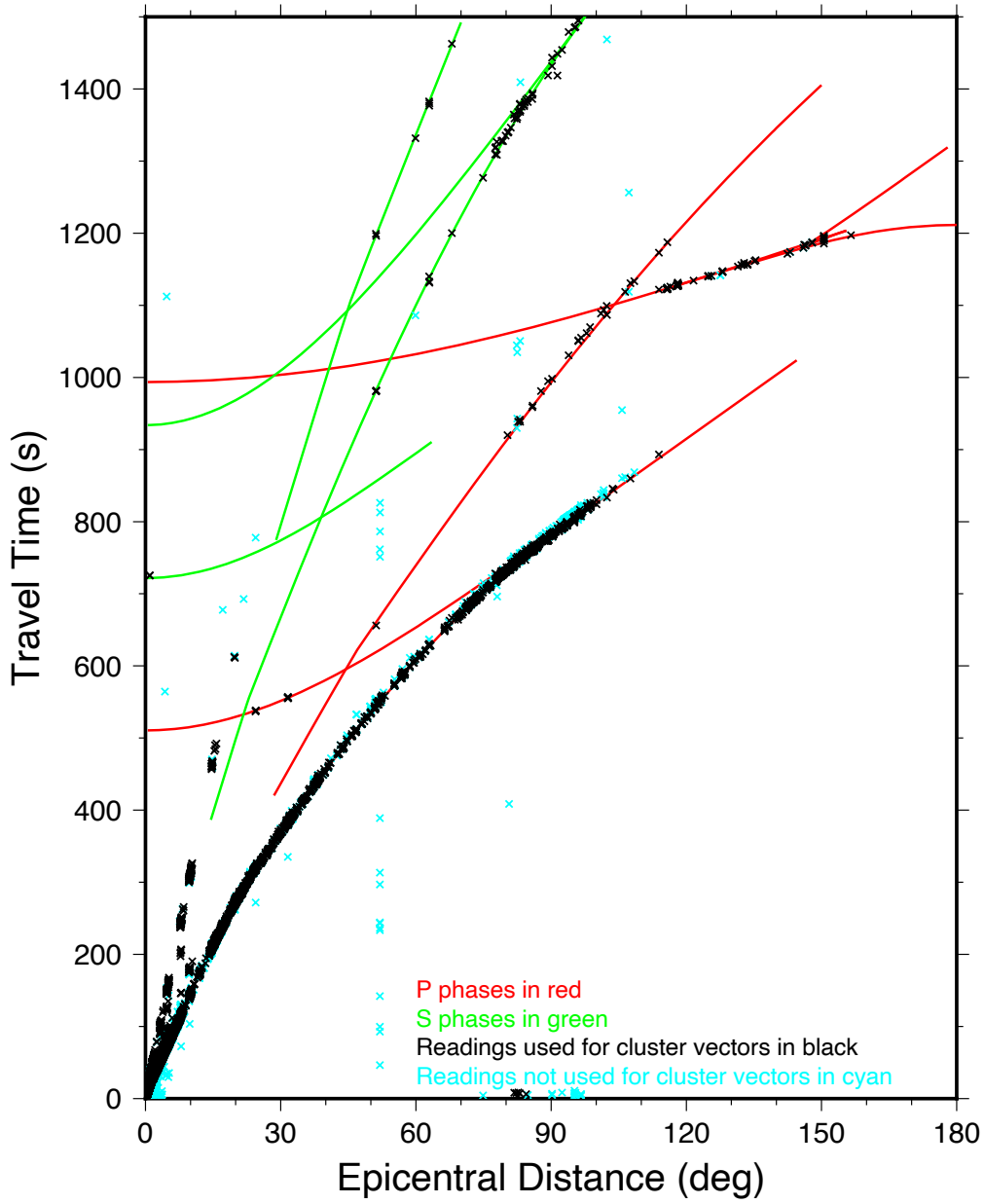| Depth range (km) | P (km/s) | S (km/s) |
|---|---|---|
| 0.00–10.00 | 5.90 | 3.30 |
| 10.00–30.00 | 6.35 | 3.65 |
| 30.00–77.50 | 7.950 | 4.48–4.49 |
| 77.50–120.00 | 7.95–8.05 | 4.49–4.50 |

July 15, 2022, 11:22pm

**Figure A4.**    Theoretical and observed arrival times. Theoretical curves are from the ak135 global model (Kennett et al., 1995). The cross symbols are individual arrival time data, colored by their usage in the relocation: black—travel times used for cluster vectors but not for hypocentroid; cyan—travel times neither used for cluster vectors nor hypocentroid.
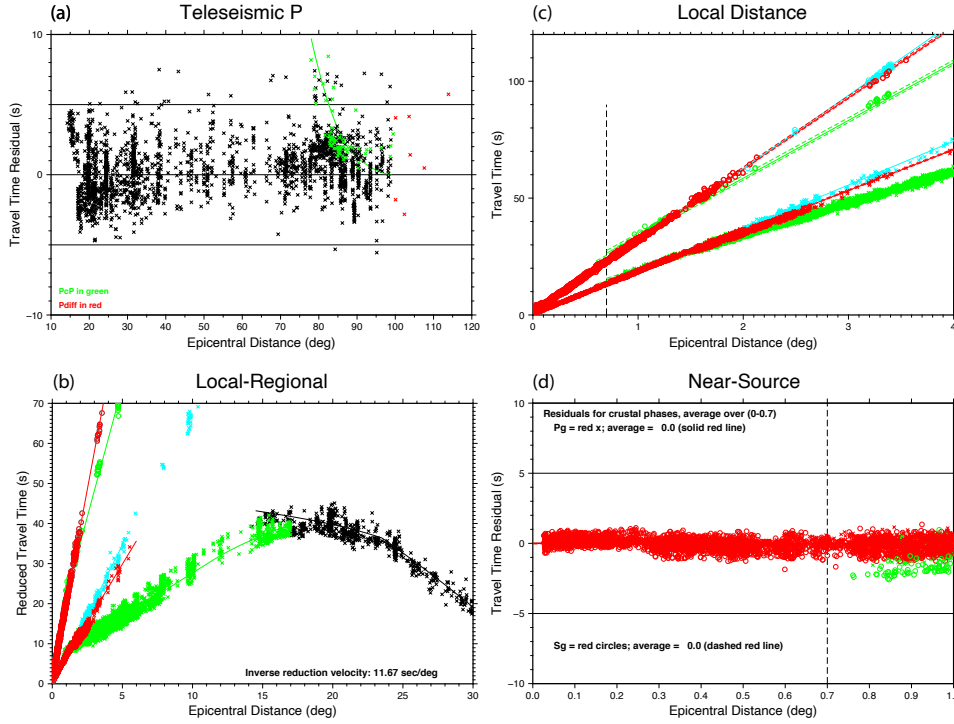
**Figure A5.** Arrival times at various epicentral distance ranges. (a) $P$ phase arrivals (black crosses) from $10°$–$120°$, reduced to the theoretical time (ak135, (Kennett et al., 1995)). The green line denotes the theoretical arrival time of phase $PcP$. (b) Travel times up to an epicentral distance of $30°$, and reduced for visual readability (11.67 seconds/degree in inverse form, or 350 seconds at $30°$). The phases include: red crosses—$Pg$ and $Sg$; blue crosses—$Pb$ and $Sb$; green crosses—$Pn$ and $Sn$; black crosses—$P$; cyan circles—any other phases. (c) Travel times over $0°$–$4°$ epicentral distances. The theoretical travel times are based on the customized velocity model in Supplementary Table B1. The phases include: red crosses—$Pg$; blue crosses—$Pb$; green crosses—$Pn$; red circles—$Sg$; blue circles—$Sb$; green circles—$Sn$; cyan circles—any other phases. The vertical dashed line denotes the distance limit used to calculate the hypocentroid. (d) The residual for each arrival time within the epicentral distance used for estimating the hypocentroid, illustrated by the vertical dashed line at $0.7°$. The solid and dashed red lines represent the average travel time residual for each phase. The green circles beyond the $0.7°$ mark is phase $Sn$.

July 15, 2022, 11:22pm

**Table C1.**     Parameters of the InSAR-GNSS distributed slip model sub-fault patches. The header is row 1; the patches of the western, central, and eastern model faults span rows 2–49, 50–77, and 78–104, respectively (see Table 2 for strike, dip, and rake values for each model fault). Each patch is 2 km × 2 km. Eastings and northings refer to the central coordinates of each sub-fault patch's surface projection.

**Table C2.**     *mloc* calibrated hypocenters of the mainshock and 196 aftershocks. The relocated hypocentral values include the origin date, origin time, epicentral latitude and longitude, and focal depth. The depth code refers to the methods and/or data source of the focal depth estimation: m—mloc free parameter solution, n—near-source readings, l—local-distance readings. For free depth solutions, the uncertainties in depth are calculated from the covariance matrix of the relocation. For manually fixed depths, the uncertainties are estimated from observations and trials to be ±2 km and ±3 km for the depth codes n and l, respectively. The ellipse semi-axis azimuth (°) and length (km) reflect the uncertainties in the epicenter location. The short semi-axis azimuth is implied (perpendicular to the long semi-axis). The earthquake magnitude is gathered from the ISC bulletin and ANSS ComCat. Further information of *mloc* direct calibration output and depth constraints can be found at https://seismo.com/mloc/hdf-files/ and https://seismo.com/mloc/depth-constraint/.

**Table C3.** Regional moment tensor solutions for the 90 best-recorded events. We model the regional waveforms and invert for the moment magnitude, centroid depths, the six moment tensor components, and the two possible nodal planes of the focal mechanism. The origin date, origin time, and epicentral latitude and longitude are gathered from NEIC. The moment tensor components (mrr, mtt, mpp, mrt, mrp, mtp) are in N m units. The last column ('source') refers to the data source (us—NEIC; nn—UNR) and phase type used in the inversion (Mwr—whole seismogram; Mww—W-phase). See Section 3.4 for full details of the waveform modeling.